Supplementary information

High-resolution remotely sensed evidence shows solar thermal power plant increases grassland growth on the Tibetan Plateau

Naijing Liu[1,2], Huaiwu Peng[1,*], Zhenshi Zhang[1], Yujin Li[1], Kai Zhang[3], Yuehan Guo[1], Yuzheng Cui[4], Yingsha Jiang[1], Wenxiang Gao[1], Donghai Wu[5]

[1]POWERCHINA Northwest Engineering Corporation Limited, Xi'an 710065, China

[2]State Key Joint Laboratory of Environmental Simulation and Pollution Control, School of Environment, Beijing Normal University, Beijing 100875, China

[3]Department of Geography and Resource Management, The Chinese University of Hong Kong, Hong Kong 999077, China

[4]School of Geography and Tourism, Shaanxi Normal University, Xi'an 710119, China

[5]Key Laboratory of Vegetation Restoration and Management of Degraded Ecosystems, and Guangdong Provincial Key Laboratory of Applied Botany, South China Botanical Garden, Chinese Academy of Sciences, Guangzhou 510650, China

*Corresponding authors: penghuaiw@nwh.cn (Huaiwu Peng).

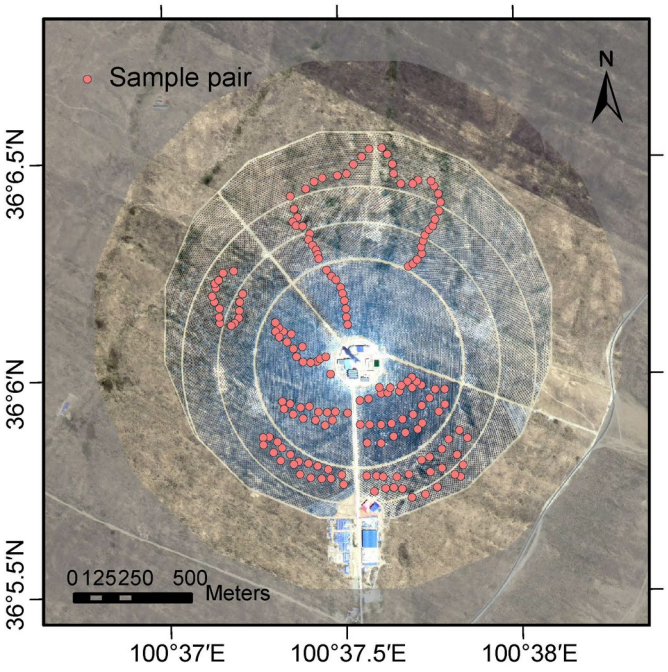


Figure S1. In-situ sample pairs at the Gonghe solar thermal power plant.

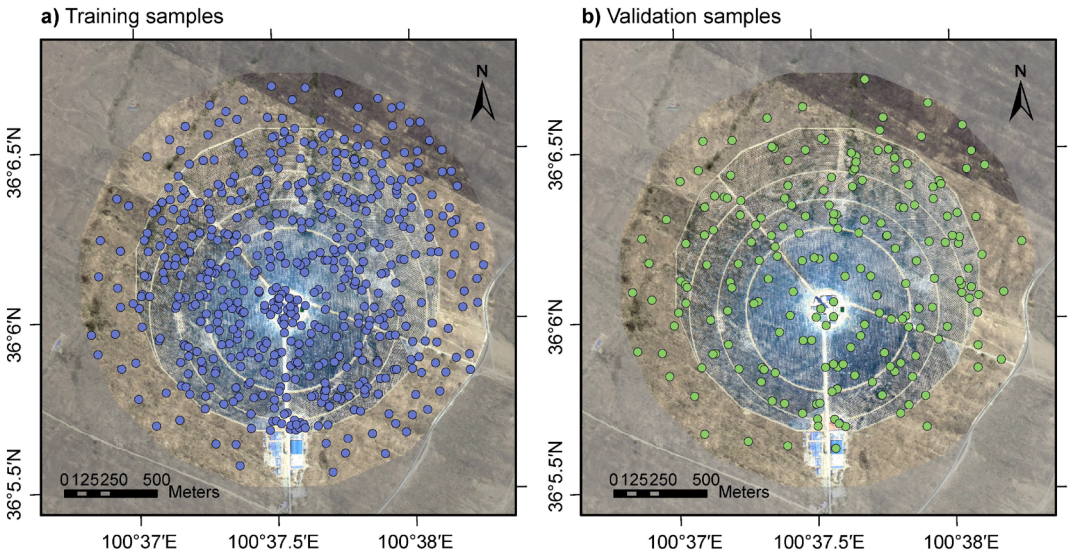


Figure S2. Training and validation samples for soft voting classification method in this study.

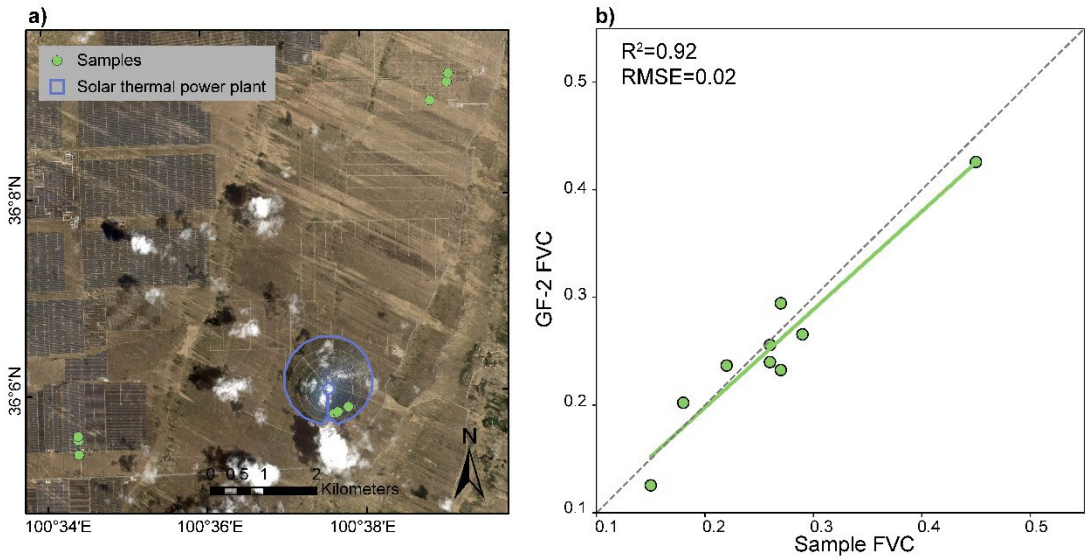


Figure S3. Assessment of GF-2 FVC through in-situ sampling. a) Depicts the geographic distribution of evaluation samples, and b) illustrates the linear regression analysis correlating the FVC measurements from samples with those obtained from GF-2. The coefficient of determination (R^2) and Root Mean Square Error (RMSE) are indicated within the plot.

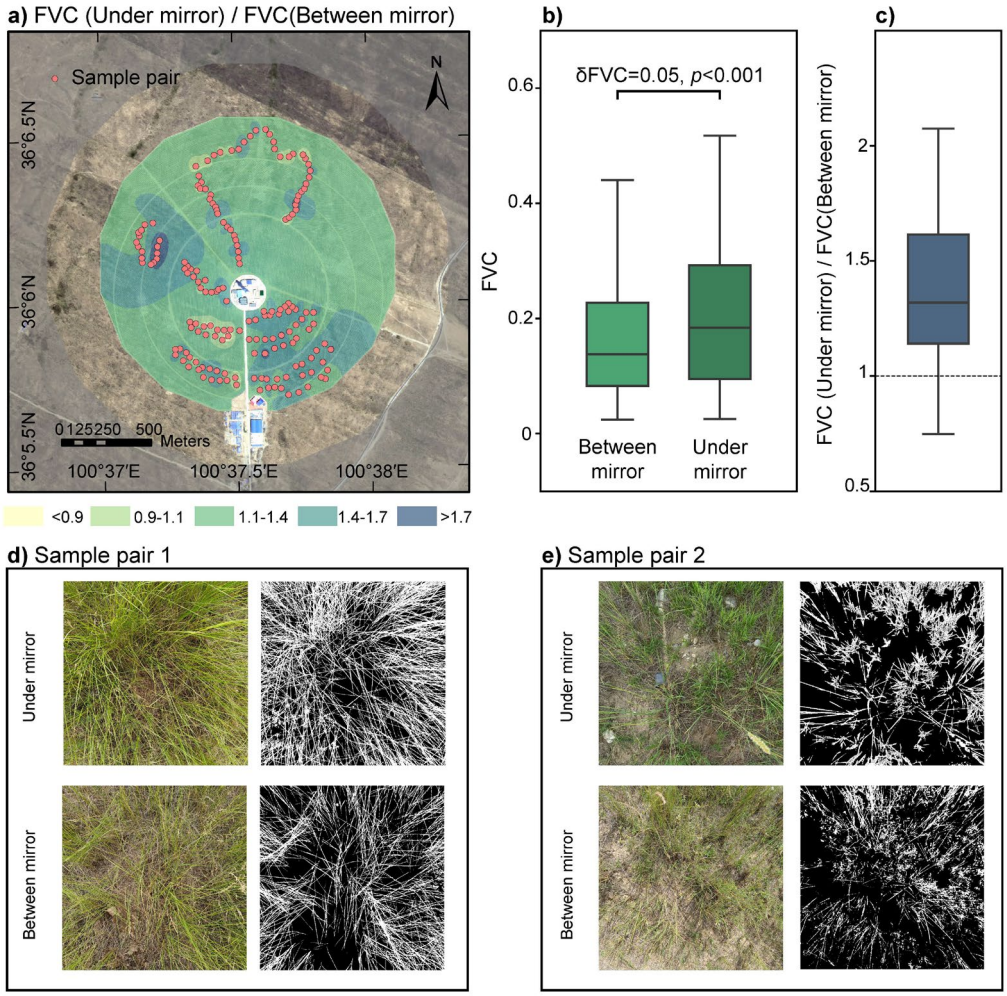


Figure S4. FVC ratio between surfaces under and between mirrors of the Gonghe solar thermal power plant. Subfigure a) illustrates the locations of in-situ sample pairs along with the spatial distribution of FVC ratios throughout the plant. Subfigure b) presents a boxplot comparing the FVC values of surfaces between and under the mirrors, with the δFVC and the results of a two-sample t-test discussed in the text. Subfigure c) displays a boxplot of the ratio of FVC values under versus between the mirrors. Subfigures d) and e) provide the FVC extraction process using RGB imagery examples of two in-situ sample pairs.

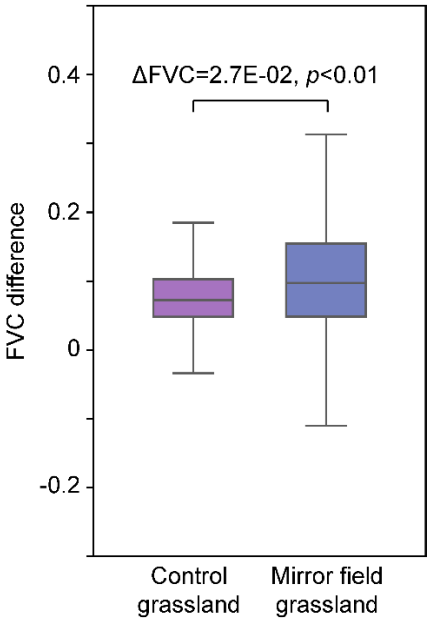


Figure S5. Boxplot illustrating the differences in grassland FVC between the mirror field and the control region. The ΔFVC values are presented, along with the statistical significance of the two-sample t-test as shown in the accompanying text.

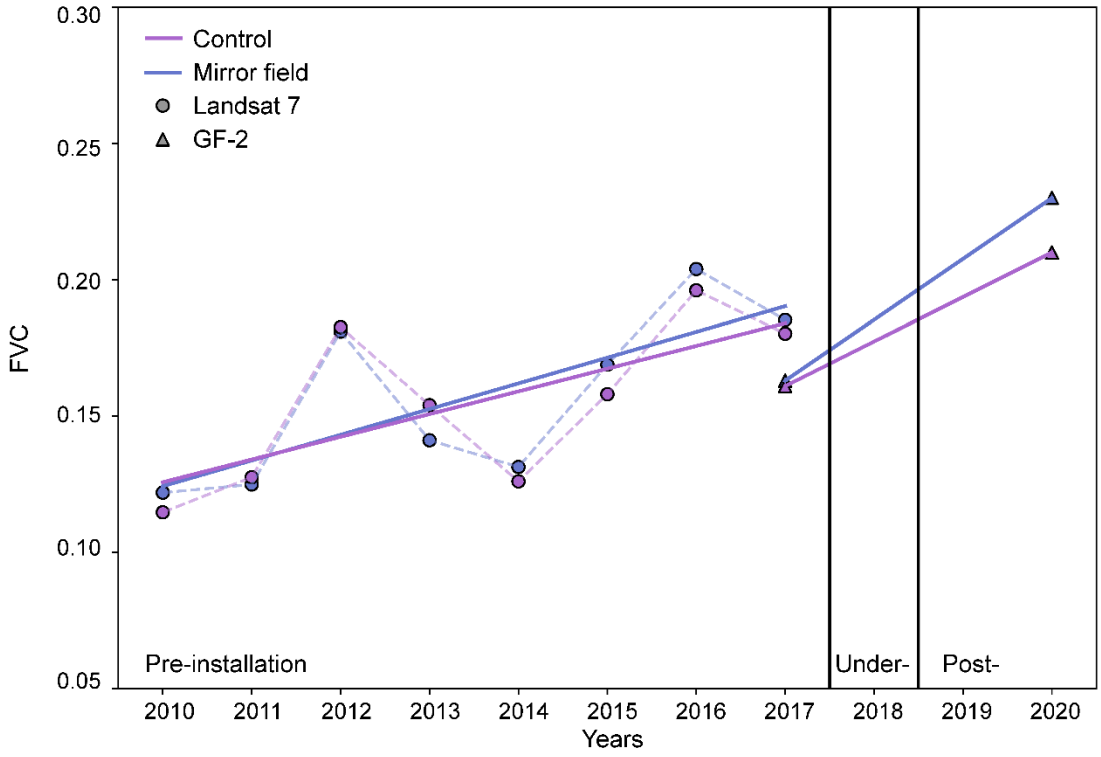


Figure S6. Time series of FVC from Landsat 7 and GF-2 spanning the years 2010 to 2020. The linear regression analyses of the time series data are represented by solid

lines.

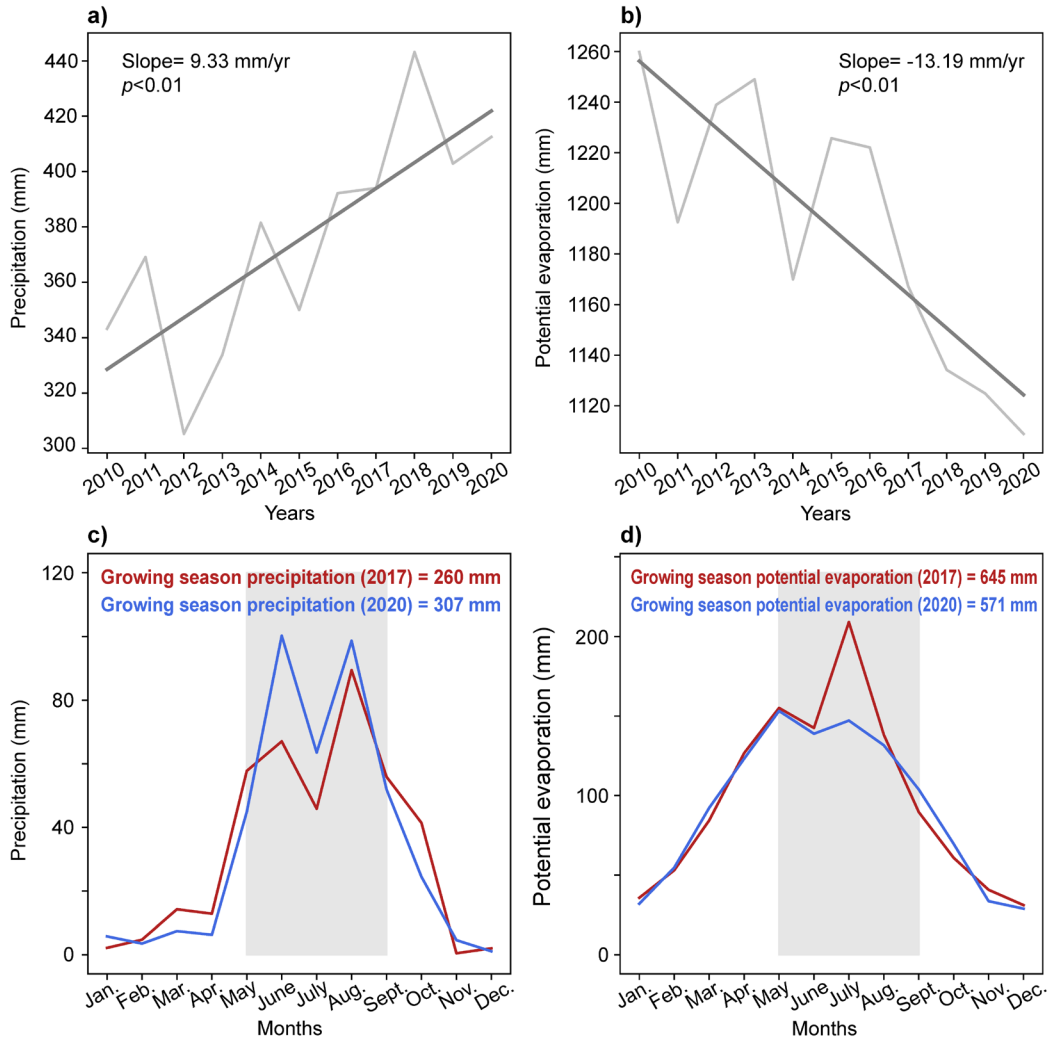


Figure S7. Time series of ERA5 Land precipitation and potential evaporation of the Gonghe solar thermal power plant. Subfigures a) and b) display the inter-annual time series of ERA-5 Land precipitation and potential evaporation, respectively, from 2010 to 2020. The slopes of the trends and their statistical significance are discussed in the text. Subfigures c) and d) illustrate the monthly time series of ERA5 Land precipitation and potential evaporation for the years 2017 and 2020, represented in red and blue, respectively. Additionally, the average precipitation and potential evaporation during the growing season (May to August) are provided in the text.

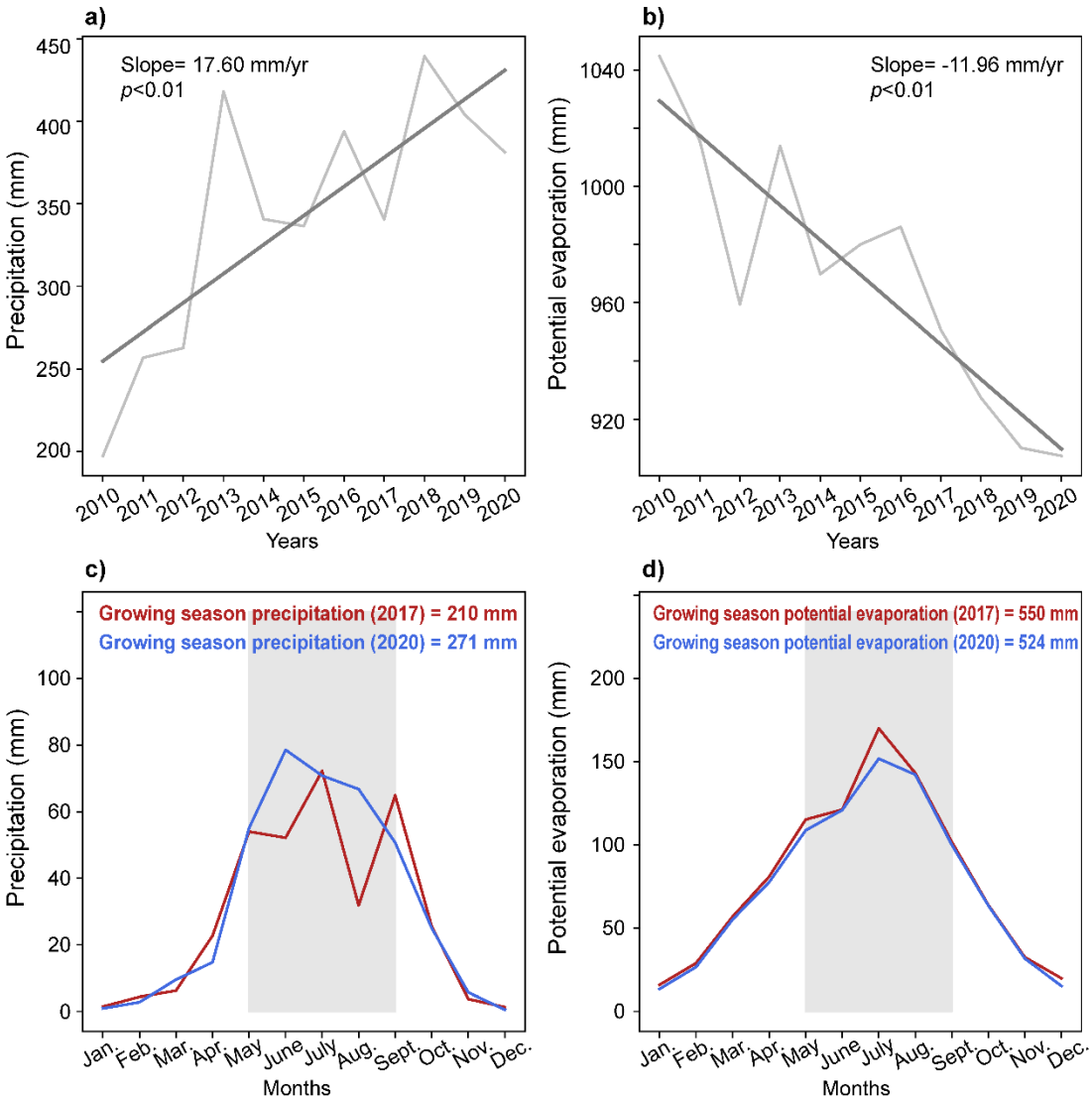


Figure S8. Time series of 1-kilometer precipitation and potential evaporation of the Gonghe solar thermal power plant. Subfigures a) and b) display the inter-annual time series of 1-kilometer precipitation and potential evaporation, respectively, from 2010 to 2020. The slopes of the trends and their statistical significance are discussed in the text. Subfigures c) and d) illustrate the monthly time series of 1-kilometer precipitation and potential evaporation for the years 2017 and 2020, represented in red and blue, respectively. Additionally, the average precipitation and potential evaporation during the growing season (May to August) are provided in the text.